# Temperature Prediction Study of Graphite Purification Zone in Arc Plasma Based on Intelligent Algorithm

# Ying Wang<sup>1</sup>, Jinmao Li<sup>1</sup>, Yan Zhang<sup>1</sup>, Rui Huang<sup>1</sup>, Chunlian Song<sup>2,\*</sup>

<sup>1</sup>School of Electrical and Information Engineering, Heilongjiang University of Technology, Jixi, China <sup>2</sup>Plasma Biomass Materials Research and Testing Provincial Laboratory, Heilongjiang University of Technology, Jixi, China

\* Corresponding author.

#### **Abstract**

Predicting the temperature in the graphite purification zone of arc plasma is not only useful for guiding the smoothness of the production process, which affects the final quality of the graphite product, but also provides decision support for the implementation of fine temperature control. This study conducted an analysis of nine variables associated with the temperature of the graphite purification zone within arc plasma to develop temperature prediction models. Using the random forest algorithm for feature selection, four key variables were identified with importance exceeding 0.4. These variables include the main gas flow rate, powder flow rate, voltage, and current. Subsequently, three different algorithms, namely Error Back Propagation (BP), Extreme Learning Machine (ELM), and Long Short-Term Memory (LSTM), were employed to develop various models for predicting temperature. Ultimately, the predictive performance of the models was assessed by comparing the temperature prediction models for various operating scenarios using different evaluation criteria. The experimental results show that the three models have their own advantages and disadvantages in different working conditions. The LSTM model exhibited superior predictive performance in C1~C2 and C6~C9 working conditions, the ELM model demonstrated superior predictive performance in C3~C4 working conditions, and the BP model demonstrated superior predictive performance in C5 working conditions. Hence, in the actual purification process, a variety of prediction models can be used in combination to facilitate the continuous monitoring of temperature variations in the graphite purification zone.

**Keywords:** Arc plasma, Graphite purification, Temperature prediction models, Intelligent algorithms, Random forests.

#### 1. Introduction

Intelligent algorithms can make predictions and inferences by learning patterns between inputs and outputs without any prior knowledge of the inner workings of the system, but rather use their "black box" nature to train the constructed multiple hidden layers with the aid of massive amounts of data, and automatically learning features from the data to quickly deal with a variety of complex, highly non-linear problems. Currently, intelligent algorithms are widely used in the field of materials manufacturing [1-4].

Common high-temperature graphite purification method requires high purity of raw materials, the carbon content must reach more than 99%, purification operation technology is not only strict requirements, need to isolate the air, and expensive equipment, huge investment [5,6]. At present, Professor Song Chunlian's team at the Provincial Plasma Key Laboratory at Heilongjiang University of Technology and the Faculty of Science of Dalian Maritime University have jointly conducted research to build an arc plasma graphite purification system,

which has important applications in the field of graphite purification technology. This method can be used to purify graphite raw materials by gasifying the impurities in the graphite raw materials using an arc plasma discharge environment at a lower cost than the high temperature physical purification method [7,8]. Temperature is the key performance index of arc plasma purification, which can be regulated by changing parameters such as current and voltage.

Intelligent algorithms can be applied to the arc plasma graphite purification process to realize the prediction of the temperature in the graphite purification zone by preprocessing, training and learning from a large amount of purification process data. This approach facilitates the smooth control of the production process and ensures the quality of the graphite purification process. In this study, the random forest algorithm was employed for feature selection of input variables. This was followed by the utilization of three distinct algorithms — error back propagation (BP), Extreme Learning Machine (ELM), and Long Short-Term Memory network (LSTM) — to develop various temperature prediction models. Various assessment criteria were subsequently applied to evaluate the effectiveness of the models. The temperature prediction model studied in this study is mainly applied to the design and development of discharge plasma graphite purification equipment, which on the one hand offers decision support for precise temperature regulation within the graphite purification zone. On the other hand, the theoretical foundation for the continuous innovation and development of plasma graphite purification technology.

#### 2. Research Base

# 2.1 Main equipment and layout of graphite purification zone

The main power supply, purification reactor, graphite powder feed equipment, refrigeration equipment, working gas delivery system together with the main-control center form the arc plasma graphite purification equipment. The main power supply on the one hand provides energy, and on the other hand with the main-control center through the voltage, current, main gas flow, and other parameters of regulation and control to generate arc plasma in conjunction with the main-control center. Subsequently, the graphite powder is purified through the powder feed device to the arc lance mouth for purification [9,10]. The main equipment and layout of the graphite purification area are shown in Fig. 1. In Fig. 1, 1 is an infrared thermometer of model IMPACMB35L, 2 is a spray gun, and the grid-like container located under the spray gun port is a graphite recovery device. The temperature of the DC arc of this device ranges from 800 degrees Celsius to 3000 degrees Celsius, depending on the intensity of the arc, current, voltage, and other factors. Therefore, the graphite purification device can realize graphite purification by setting and controlling the voltage, current and other parameters.



Fig. 1. Main equipment and layout of graphite purification zone

#### 2.2 Analysis of factors affecting the temperature of graphite purification zone

The temperature within the graphite purification zone of the arc plasma is primarily determined by the arc. Various factors influence the arc temperature, including the current, voltage, working gas flow, gas type, physical characteristics of the material being purified, environmental conditions, and other relevant parameters.

ISSN: 1750-9548

Cheng Manqing et al. analyzed and calculated the variation of the arc temperature field when the current conditions were changed. The results were clear: the arc temperature values vary with the current. The radial current density and axial current density in the arc zone increase with the current increment, and the arc temperature values were directly proportional to the current [11]. Du Huayun et al. analyzed and studied the effects of changes in protective gas flow and arc length conditions on the arc temperature field and flow field. Their results showed that under the same current conditions, the maximum temperature increased with the increase in arc length. And with other conditions remaining unchanged, the maximum arc temperature demonstrated a rising trend followed by a subsequent decline as the flow rate of the protective gas was augmented [12]. Chai Tongtong et al. used ANSYS software to analyze the numerical simulation of argon and helium plasma arcs. Through comparison, they found that the peak temperature of the argon arc temperature field was greater than that of the helium arc temperature field. However, because the larger area occupied by the high-temperature region of the helium arc, the average temperature value of the helium arc temperature field was actually higher than that of the argon arc temperature field [13]. Wang Dongsheng et al. showed that the thermophysical parameters of the material have a crucial influence on the calculation of the temperature field. According to the principles of heat conduction theory, it can be established that the process of thermal energy exchange between entities is instigated by differences in their respective temperatures, and there is heat exchange between plasma and powder at the surface of the powder [14]. Zhou Yan et al. analyzed the effects of environmental factors on the operational characteristics of a synthetic plasma jet exciter. They demonstrated that variations in environmental factors also influence the arc temperature, for example, the ambient air pressure and temperature [15].

Therefore, in practice, it is necessary to consider the extent to which these factors affect the arc plasma graphite purification zone's temperature. By optimising the arc parameters and equipment design, the stability of the arc can be improved, resulting in a desirable purification temperature. The study of the primary factors influencing the temperature change process in the graphite purification zone and the investigation of the establishment of the corresponding temperature prediction model are also necessary to realize the study of the temperature prediction control system, as they are based on the full utilization of the actual production data.

# 3. Research Methodology

#### 3.1 Data acquisition

In conjunction with the aforementioned analysis, nine variables affecting the temperature in the graphite purification zone were identified during the experiments. These variables include the main gas flow, powder feed flow, cooling water temperature, ambient temperature, voltage, current, ambient humidity, ambient air pressure, and graphite purification zone temperature. For the sake of analysis, each variable is abbreviated and defined in Table 1.

Table 1. Description of variables related to the temperature in the graphite purification zone

No.	Variable	Unit	Scope of change	Variable abbreviation
1	Main gas flow	L/min	[20~25]	F1
2	Powder feed flow	g/min	[80~100]	F2
3	Cooling water temperature	$^{\circ}\mathrm{C}$	[5~6]	F3
4	Ambient temperature	$^{\circ}\mathrm{C}$	[29~31]	F4
5	Voltage	V	[27~30]	V
6	Current	A	[200~500]	A
7	Ambient humidity	%	[60~69]	RH
8	Ambient air pressure	kPa	[97.9~98.0]	P
9	Graphite purification zone temperature	$^{\circ}\mathrm{C}$	[851.2~2089.1]	Т

ISSN: 1750-9548

The experimental data were obtained from the plasma graphite purification equipment at the Provincial Plasma Key Laboratory at Heilongjiang University of Technology. A total of 4,500 data sets were collected for the situation within 2100 degrees Celsius, including nine working conditions, each containing 500 data sets. The lowest temperature point in the graphite purification zone was selected as the measurement point, and the working conditions were set according to the conclusions of the previous laboratory research. The original data conditions are detailed in Table 2. It shows that the temperature fluctuation value is significant in the graphite purification environment due to its complexity. Furthermore, under the same working condition, the temperature range can exceed 200 degrees Celsius, indicating a substantial disparity between the lowest and highest recorded temperatures. Consequently, prior to utilising the actual data, it is imperative to perform outlier testing on the data to reduce the impact of such data on the model, which is conducive to improving the accuracy of the temperature prediction model.

Table 2. Nine working conditions

Working conditions	C1	C2	C3	C4	C5	C6	C7	C8	C9
F1(L/min)	20	25	25	25	25	25	25	30	20
$range(\pm 1\%)$ F2(g/min) $range(\pm 1\%)$	100	90	80	100	100	100	80	90	90
F3(°C)	6	6	6	6	6	7	7	7	7
F4(°C)	30	30	30	30	30	30	30	31	31
V(V) range(±1%)	24	30	25	29	28	27	28	29	28
A(A) range(±1%)	200	300	300	400	250	200	500	500	500
RH(%)	61	61	61	61	61	61	62	62	62
P(kPa)	97.9	97.9	97.9	97.9	97.9	97.9	97.9	98	98
T(°C)	853.3	1729.7	1619.9	1831.9	1534.6	1424	1947.8	1636.2	1997.3
1( C)	~872.5	~1909.9	~1845.2	~2010.8	~1717.1	~1549.5	~2002.9	~1853.4	~2090.8

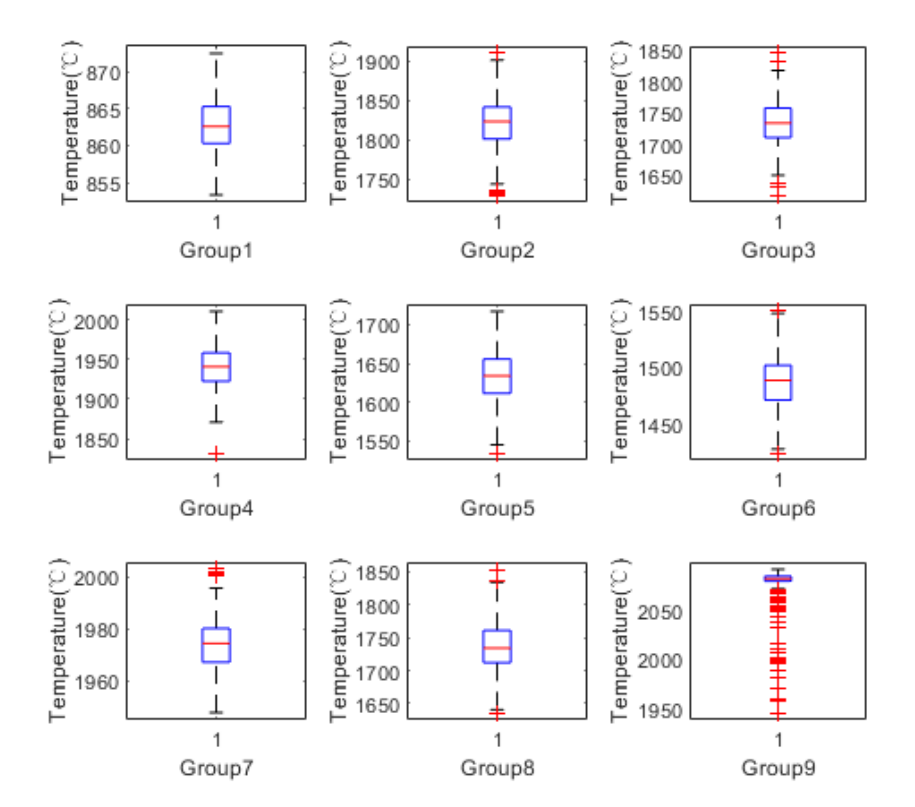


Fig. 2. Box plots for handling outliers

#### 3.2 Data pre-processing

Data pre-processing included outlier removal, normalisation and analysis of variable significance. Box plots are used for outlier removal. A box plot is a graph used to show the centre position and range of dispersion of one or more groups of continuous data distribution, which can show the main statistical information such as the median, quartile and outliers of the data, and is named box plot because of its resemblance to a box [16,17]. The median of the data, which is the central line of the box, signifies the average of the data within the selected sample set. The top line of the box represents the upper quartile of the data, while the bottom line represents the lower quartile. The extent of the alteration in the data can be demonstrated by the height of the box. The graphite purification zone temperatures for the nine working conditions are plotted on their respective box plots as shown in Fig. 2, where the data between the top and bottom edges can be used normally, while the discrete points (outliers) beyond them are eliminated by mean replacement.

Before training the temperature model, the data must also be normalised, and it can be seen from the information in Table 1 that the production data should be normalized before use because it contains data with different dimensions, such as temperature and pressure. Normalization can address the issue of the loss of data expression characteristics due to differing dimensions, which can affect the accuracy of the prediction model. Furthermore, normalization can accelerate the convergence speed of the model. Consequently, the original data are mapped to the [0,1] range for dimensionless processing by employing the min-max method [18].  $x_i$  represents the ith data of this set of variables. The minimum value within the set of variables is represented by  $x_{min}$ , while the maximum value is represented by  $x_{max}$ , and  $\hat{x}$  is the normalised data.

$$\hat{x} = \frac{x_i - x_{\min}}{x_{\max} - x_{\min}} \tag{1}$$

In addition, to simplify computational sophistication, this study utilizes the Random Forest algorithm to evaluate the input factors and determine their relative importance. The results of this analysis are presented in Fig. 3. Input variables with a significance level below 0.4 were eliminated, and it was ultimately determined that the variables of main gas flow (F1), powder feed flow (F2), voltage (V), and current (A) would be utilized as inputs to the temperature prediction model.

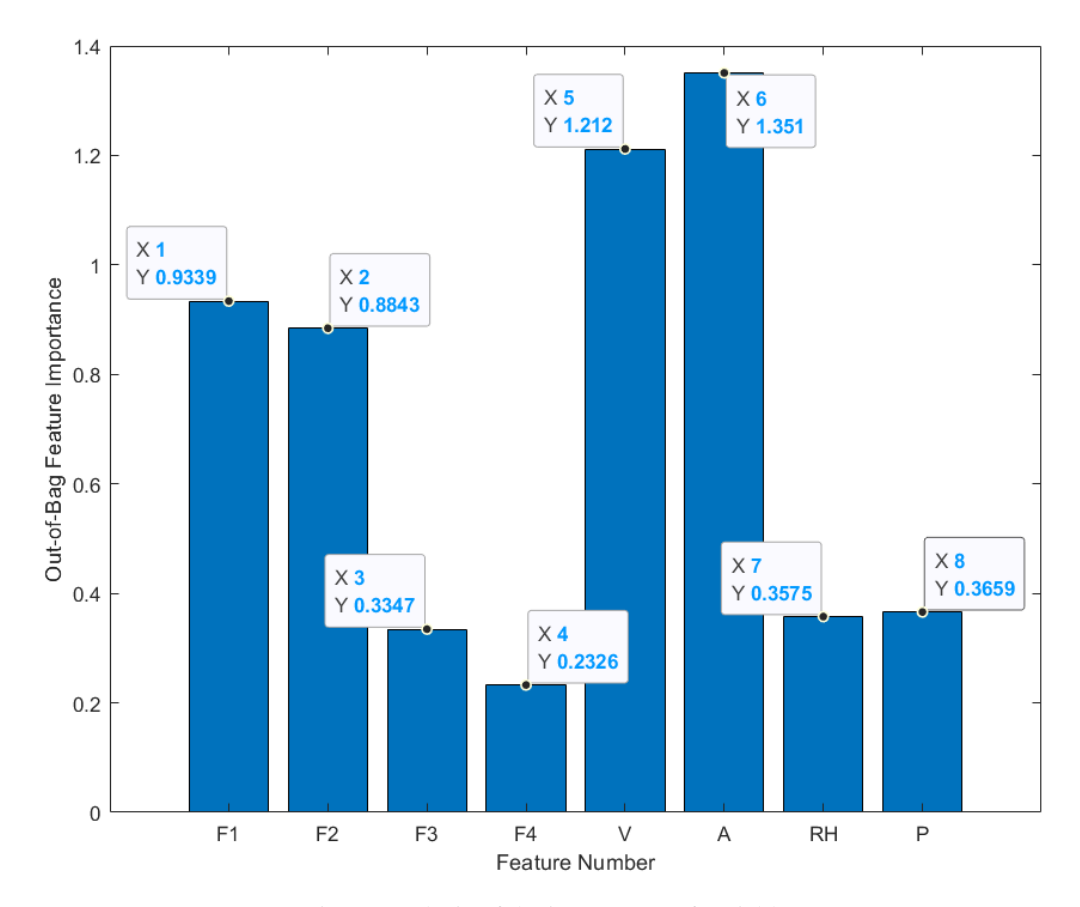


Fig. 3. Analysis of the importance of variables

#### 3.3 Model of the BP algorithm

To realize the learning and training of the BP network by continuously adjusting the weights of each layer and gradually reducing the difference in the output value and the expected value during signal and error propagation. The neurons in the hidden layer act as receivers of the input signal, responsible for processing and transmitting it to the next layer. When the neurons in the final layer have completed their processing, the forward propagation of learning is complete. If the calculated error between the actual output and the desired output is found to be unsatisfactory up to the set requirement, back propagation of the error signal is performed [19].

Assuming that the hidden layer is a single layer, let the overall structure of the BP model be n-m-k, where n, m, and k represent the number of neurons in the corresponding layer. The symbols  $\omega_{ji}$  represent the weights that connect the first layer to the neurons in the hidden layer, while  $b_j$  represent the thresholds that exist between these respective layers. The symbols  $v_{kj}$  denote the weights linking the neurons of the hidden layer to those of the final layer, while  $c_k$  represent the thresholds that exist between these respective layers.

The activation value  $h_j$  of the hidden layer neuron, and the activation value  $y_k$  of the output neuron are calculated as follows:

$$h_j = \sum_{i=1}^n \omega_{ji} x_i + b_j \tag{2}$$

$$y_k = \sum_{j=1}^m v_{kj} \sigma(h_j) + c_k \tag{3}$$

The tansig function is selected as the activation function of  $\sigma(h_j)$ , with the purelin linear function is selected as the activation function of the output neurons. This is incorporated into the error function E after calculating  $h_j$  and  $y_k$ , where  $t_k$  denotes the output target.

ISSN: 1750-9548

$$E = \frac{1}{2} \sum_{k=1}^{k} (y_k - t_k)^2 \tag{4}$$

In accordance with the error function E, the weights  $v_{kj}$  are adjusted during back propagation. Let  $\delta_k$  be the neuron error of the output layer, where  $\sigma'(h_i)$  is the derivative of the tansig function:

$$\delta_k = (y_k - t_k)\sigma'(h_i) \tag{5}$$

According to the chain rule, the gradient of  $v_{kj}$  is:

$$\frac{\partial E}{\partial v_{kj}} = \frac{\partial E}{\partial y_k} \frac{\partial y_k}{\partial v_{kj}} = \delta_k \sigma(h_j)$$
 (6)

Set  $\eta$  as the learning rate. The weights of  $v_{ki}$  and  $\omega_{ii}$  can be updated by gradient descent:

$$v_{kj} = v_{kj} - \eta \frac{\partial E}{\partial v_{kj}} \tag{7}$$

$$\omega_{ji} = \omega_{ji} - \eta \frac{\partial E}{\partial \omega_{ji}} \tag{8}$$

Substituting  $\delta_k$  into the calculation gives the hidden layer neuron error  $\delta_{kj}$ :

$$\delta_j = \sigma'(h_j) \sum_{k=1}^k \delta_k \nu_{kj} \tag{9}$$

The thresholds of  $b_i$  and  $c_k$  are modified in the following manner:

$$b_j = b_j - \eta \delta_j \tag{10}$$

$$c_k = c_k - \eta \delta_k \tag{11}$$

# 3.4 Model of the ELM algorithm

The ELM algorithm is the random initialization of the input layer's weights and thresholds, without adjusting them during the training process, while the weights for the output layer are computed by generalized inverse matrix theory. The approach does not require the use of complicated optimization algorithms, such as backpropagation algorithms, to modify the network weights. This leads to quicker training and enhanced generalization of the ELM. In addition, ELM can handle high-dimensional data and non-linear problems, but in practical applications, regularisation strategies are also needed to avoid overfitting problems [20,21].

The ELM algorithm randomly sets connection weights  $\beta_i$  after determining the quantity of hidden layer neurons. Subsequently, the training data is mapped to the neuron  $l_i$ .

$$L = \begin{bmatrix} l_1(x_1) & l_2(x_1) & \cdots & l_N(x_1) \\ l_1(x_2) & l_2(x_2) & \cdots & l_N(x_2) \\ \cdots & \cdots & \cdots & \cdots \\ l_1(x_m) & l_2(x_m) & \cdots & l_N(x_m) \end{bmatrix}$$
(12)

The matrix of output weight is denoted by  $\alpha$ .  $L^+$  is the pseudo-inverse matrix of L, and the target matrix of the training data is denoted by Y.

$$\alpha = L^{+}Y \tag{13}$$

## 3.5 Model of the LSTM Algorithm

LSTM is an acronym for Long Short-Term Memory. Its basic components are cell states and gate architectures. The cellular state can be conceptualized as a pathway for information transfer, which enables the sequential transmission of information. LSTM is also capable of processing different types of sequence data at high

ISSN: 1750-9548

training speeds and with high accuracy. The algorithm consists of three gates: forgetting gate, input gate and output gate, which are represented by  $z_i$ ,  $z_i$  and  $z_o$  respectively [22,23].

$$z_f = \sigma(\omega_f \cdot [y_{t-1}, i_t] + c_f) \tag{14}$$

$$z_i = \sigma(\omega_i \cdot [y_{t-1}, i_t] + c_i) \tag{15}$$

$$\widetilde{U}_t = \tanh(\omega_c \cdot [y_{t-1}, i_t] + c_c) \tag{16}$$

$$z_o = \sigma(\omega_o \cdot [y_{t-1}, i_t] + c_o) \tag{17}$$

 $\widetilde{U}_t$  is the temporary cell state.  $\omega_f$  and  $c_f$  represent the forgetting gate's weight matrix and bias vector.  $\omega_i$  and  $c_i$  represent the input gate's weight matrix and bias vector.  $\omega_c$  and  $c_c$  represent the temporary cell's weight matrix and bias vector.  $\omega_o$  and  $c_o$  represent the output gate's weight matrix and bias vector, respectively. The symbol  $\sigma$  signifies the application of a sigmoid function. Additionally, the notation  $[y_{i-1}, i_t]$  represents the concatenation of the  $y_{i-1}$  (previous moment's output) with the  $i_t$  (input at this moment) into a single vector.  $U_t$  represents the current state of the cell,  $y_t$  represents the output, and  $\circ$  represents the vector dot product operation.

$$U_t = z_f \circ U_{t-1} + z_i \circ \widetilde{U}_t \tag{18}$$

$$y_t = z_o \circ \tanh(U_t) \tag{19}$$

## 4. Testing and Analysis

To assess the predictive precision of the model, data from three distinct working conditions, designated as C2, C4, and C9, were selected for the experiment. A total of 200 data points were selected for each working condition. Figures 4-6 illustrate the prediction value curves and actual value curves of the LSTM, BP, and ELM models, emphasizing the discrepancies between the predicted and actual results for each model.

Under the C2 working condition, the prediction value curves of the three models are basically in line with the trends of the actual value curves, and the error range of the LSTM model is -11.87 degrees Celsius~5.978 degrees Celsius, the error range of the BP model is -17.89 degrees Celsius~4.788 degrees Celsius, and the error range of the ELM model is -25.88 degrees Celsius~17.74 degrees Celsius. Comparing the three models, the LSTM model has the smallest predicted error range.

Under the C4 working condition, the three models' prediction value curves basically agree with the trend of the actual value curves, and the error range of the LSTM model is -7.055 degrees Celsius~3.094 degrees Celsius, the error range of the BP model is -5.82 degrees Celsius~7.972 degrees Celsius, and the error range of the ELM model is -0.7987 degrees Celsius~1.194 degrees Celsius. Comparing the three models, the ELM model has the smallest predicted error range.

On the other hand, under the C9 working condition, the prediction value curves of the BP model show a large error, and the error range of the LSTM model is -1.755 degrees Centigrade~3.594 degrees Centigrade, the error range of the BP model is -15.55 degrees Centigrade~13.52 degrees Centigrade, and the error range of the ELM model is -3.109 degrees Centigrade~3.041 degrees Centigrade. Comparing the three models, the predicted error range of the LSTM model is the smallest.

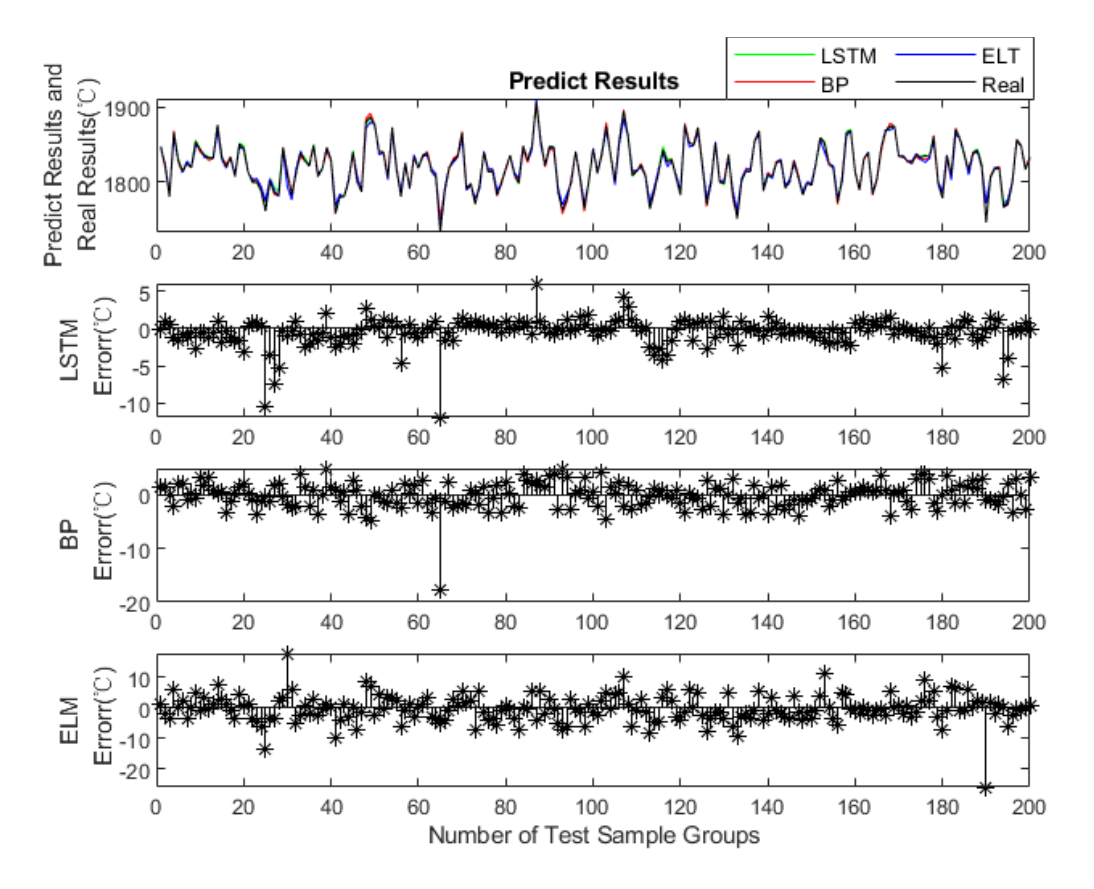


Fig. 4. Predicted results of the three algorithms under the C2 working condition

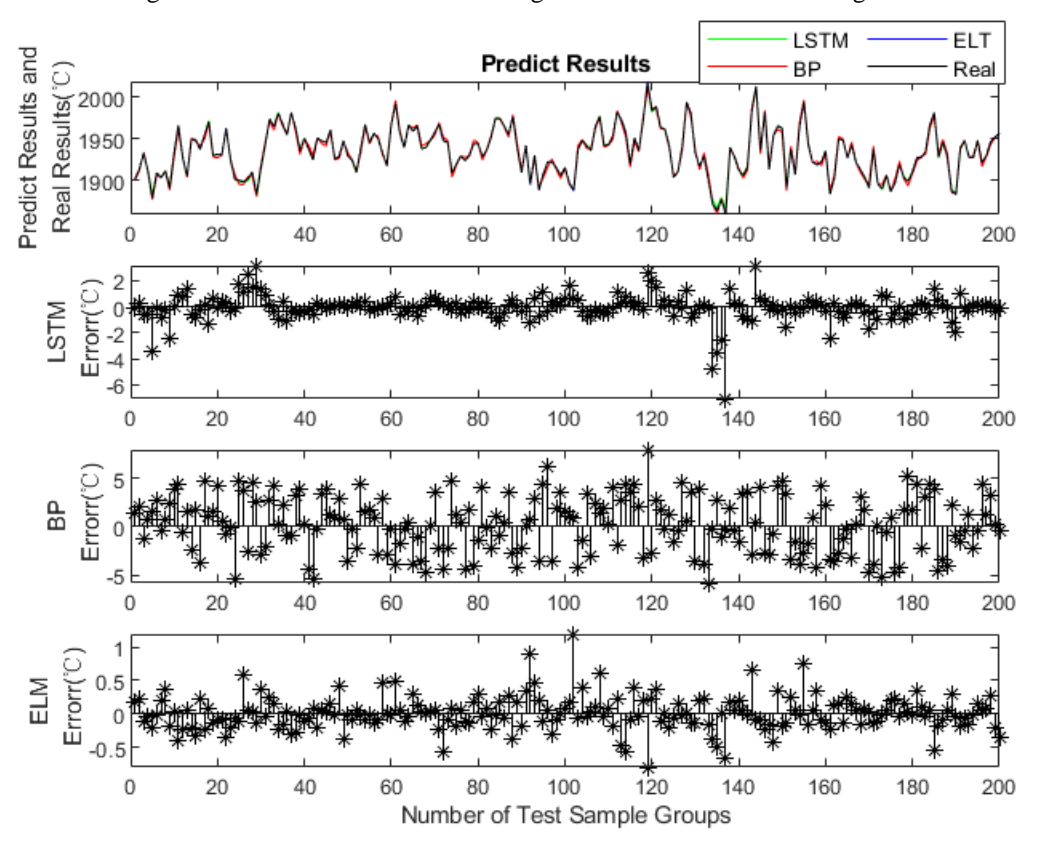


Fig. 5. Predicted results of the three algorithms under the C4 working condition

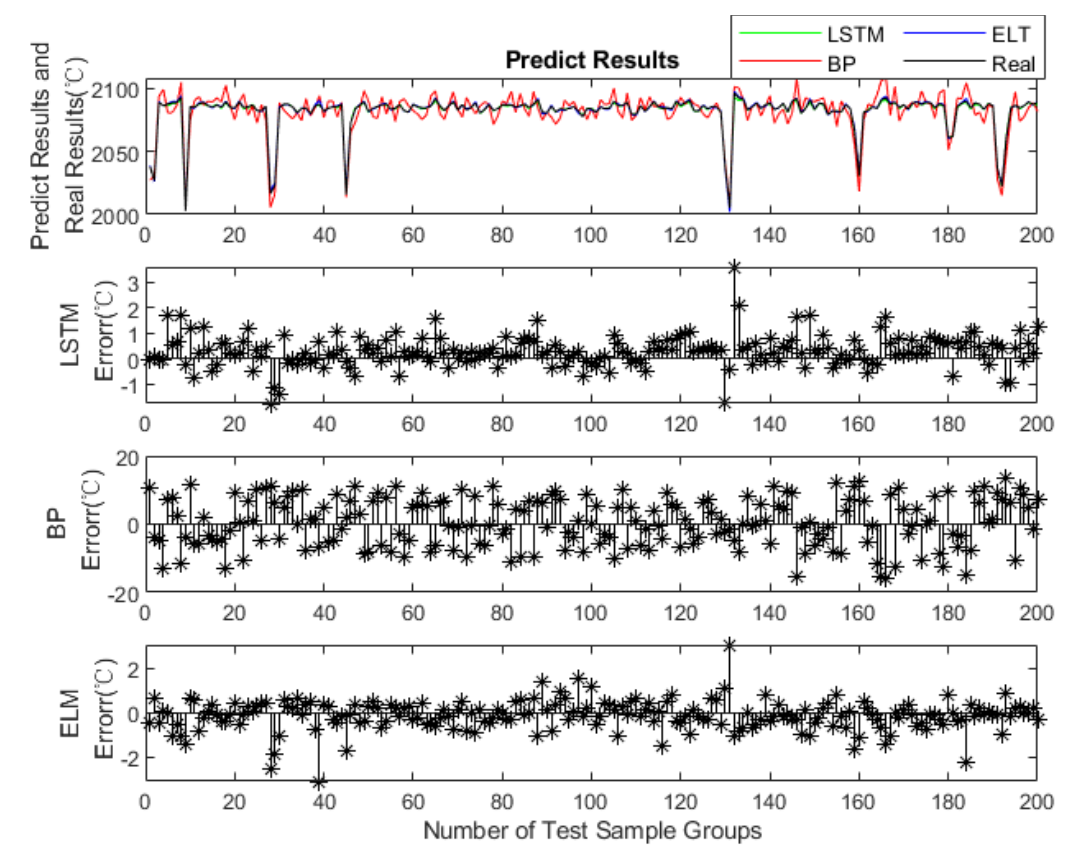


Fig. 6. Predicted results of the three algorithms under the C9 working condition  $\,$ 

Table 3. Results of evaluation indicators for different algorithms

Working condition	Evaluation indicators	BP	ELM	LSTM
	M1 (MSE)	7.9098	3.4602	1.9895
C1	M2 (MAE)	2.201	1.4828	1.0172
	M3 (MAPE)	0.0025	0.0017	0.0012
	M1 (MSE)	6.095	20.4822	3.933
C2	M2 (MAE)	1.8392	3.3052	1.2206
	M3 (MAPE)	0.001	0.0018	0.0007
	M1 (MSE)	0.6646	0.4942	1.0081
C3	M2 (MAE)	0.6875	0.5697	0.8334
	M3 (MAPE)	0.0004	0.0003	0.0005
	M1 (MSE)	8.6826	0.0645	1.1191
C4	M2 (MAE)	2.4901	0.1819	0.6314
	M3 (MAPE)	0.0013	0.0001	0.0003
	M1 (MSE)	0.938	8.6546	1.4228
C5	M2 (MAE)	0.7273	2.1936	0.8837
	M3 (MAPE)	0.0004	0.0014	0.0005
	M1 (MSE)	0.6676	0.4796	0.2902
C6	M2 (MAE)	0.4758	0.5671	0.3971
	M3 (MAPE)	0.0003	0.0004	0.0003
	M1 (MSE)	4.4604	0.7494	0.2459
C7	M2 (MAE)	1.7608	0.6128	0.3448
	M3 (MAPE)	0.0009	0.0003	0.0002
	M1 (MSE)	0.9772	2.1226	0.9614
C8	M2 (MAE)	0.7464	1.1138	0.6985
	M3 (MAPE)	0.0004	0.0007	0.0004
	M1 (MSE)	51.6591	0.4854	0.4777
C9	M2 (MAE)	6.1649	0.4973	0.5082
	M3 (MAPE)	0.003	0.0002	0.0002

ISSN: 1750-9548

To develop a deeper comprehension of the precise performance of the prediction models, different prediction models were compared under nine working conditions and analyzed using error statistics. There are three main metrics, Mean Squared Error (MSE) for metric 1, Mean Absolute Error (MAE) for metric 2, and Mean Absolute Percentage Error (MAPE) for metric 3.

$$MSE = \frac{1}{M} \sum_{j=1}^{M} (x_j - \hat{x}_j)^2$$
 (20)

$$MAE = \frac{1}{M} \sum_{i=1}^{M} \left| x_j - \hat{x}_j \right|$$
 (21)

$$MAPE = \frac{100}{M} \sum_{j=1}^{M} \frac{\left| x_j - \hat{x}_j \right|}{x_j}$$
 (22)

The variable M represents the quantity of samples contained within the test data,  $x_j$  is the actual value of the graphite purification zone temperature, and  $\hat{x}_j$  is the predicted value of the graphite purification zone temperature. All three assessment metrics share the common characteristic that as they approach zero, the model's accuracy increases and the predictive performance improves. The distinction among MSE, MAE, and MAPE lies in their respective characteristics. MSE accentuates the prediction error, exhibits greater sensitivity to outlier data, and emphasizes error values with significant impact. In contrast, the MAE places greater emphasis on the absolute value of the discrepancy between the predicted and the actual value, while MAPE gauges the relative magnitude of the deviation in terms of percentage.

Table 3 shows the results of the evaluation indices of different algorithms under nine working conditions. From the three evaluation indices, it can be seen that different algorithms have their prediction advantages and disadvantages under different working conditions. The BP model has obvious disadvantages under the C9 working condition, while it has obvious advantages under the C5 working condition; the ELM model has outstanding disadvantages under the C2 working condition, while it shows high advantages under the C3 and C4 working conditions; the LSTM model shows good predicted results under the C1~C9 working conditions, and overall the fluctuation range of the evaluation index results is the smallest. However, the model still has some shortcomings, for example, under the C2 condition, although the MSE value of the LSTM model obtained the most favorable evaluation result compared to the other two models, it is worth noting that the value is relatively high.

#### 5. Conclusion

In this study, a random forest algorithm was employed to assess the significance of characteristic variables that impact the temperature within the graphite purification zone, and finally four variables with the importance of 0.4 or more, namely, main gas flow (F1), powder feed flow (F2), voltage (V), current (A), were selected as the characteristic inputs of the temperature prediction model. Then, the three algorithms of BP, ELM and LSTM were built the prediction model, and compared the three predicted results with the actual temperature values.

The results of the study show that within the working conditions of C1~C2 and C6~C9, the LSTM model demonstrates the quality predictive performance. Under the working conditions of C3~C4, the ELM model demonstrates the quality predictive ability, and under the working conditions of C5, the BP model demonstrates the quality predictive ability. This demonstrates that under complex working conditions, although BP, ELM, LSTM and other single algorithm models can all complete the prediction of the temperature in the graphite purification zone, none of the models can have an absolute advantage, and even there are obvious disadvantages, such as the MSE of the ELM model is up to more than 20 under the C2 working condition, and the MSE of the BP model is up to more than 50 under the C9 working condition. Among them, although the predicted value curves of the LSTM model could not guarantee that the optimal predicted results were achieved under each working condition, the MSE, MAE, and MAPE evaluation indices were within 4 under nine working conditions, and the temperature prediction model constructed by this algorithm had the highest robustness compared with

the other two models. Therefore, in the actual purification process, multiple prediction models can be used in combination to more accurately realize real-time monitoring of the temperature in the graphite purification zone.

In addition, during the development of the predictive model, all operations were performed under the same experimental conditions. However, it was observed that the accuracy of the collected data could still be affected by various uncertainties, including factors such as pipeline, device structure, and environmental interference. Additionally, the restricted measurement capabilities further constrained the precision of the prediction model. Hence, further research is needed to explore methods for enhancing the precision of predictive models across various operational scenarios through advancements in data acquisition techniques and optimization of intelligent algorithms.

#### Acknowledgment

I wish to extend my heartfelt appreciation to all individuals who have played a role in the successful culmination of this research study. Furthermore, I am compelled to express my gratitude for the supported by Heilongjiang Provincial Natural Science Foundation of China "Optimised Design and Study of a DC Arc Graphite Purification Plant" (Project No: LH2021E106), and the Special Fund Project of the Basic Scientific Research Operating Expenses of Undergraduate Universities of Heilongjiang Province in 2021 "Research on Optimization of Plasma Spraying powder feed System." Their provision of necessary resources and facilities greatly contributed to the successful advancement of this research.

#### References

- [1] A. Hürkamp, S. Gellrich, T. Ossowski, J. Beuscher, S. Thiede et al., "Combining Simulation and Machine Learning as Digital Twin for the Manufacturing of Overmolded Thermoplastic Composites," Journal of Manufacturing and Materials Processing, vol. 4, Sept. 2020, pp. 92, doi:10.3390/jmmp4030092.
- [2] G. Konstantopoulos, E. P. Koumoulos, and C. A. Charitidis, "Digital Innovation Enabled Nanomaterial Manufacturing; Machine Learning Strategies and Green Perspectives," Nanomaterials, vol. 12, no. 15, Aug. 2022, pp. 2646, doi:10.3390/nano12152646.
- [3] F. Islam, C. Wanigasekara, G. Rajan, A. Swain, and B. G. Prusty, "An Approach for Process Optimisation of the Automated Fibre Placement (AFP) Based Thermoplastic Composites Manufacturing Using Machine Learning, Photonic Sensing and Thermo-Mechanics Modelling," Manufacturing Letters, vol. 32, Apr. 2022, pp. 10-14, doi:10.1016/j.mfglet.2022.01.002.
- [4] J. Fernández-León, K. Keramati, D. Garoz, L. Baumela, C. Miguel et al., "A Machine Learning Strategy for Race-Tracking Detection During Manufacturing of Composites by Liquid Moulding," Integrating Materials and Manufacturing Innovation, vol. 11, no. 2, June 2022, pp. 296-311, doi:10.1007/s40192-022-00263-6.
- [5] Z. Ling, W. Jiang, J. Shao, and X. Liu, "Experimental study on preparation of high purity graphite by high-temperature roasting," Non-Metallic Mines, vol. 43, no. 01, Jan. 2020, pp. 37-39.
- [6] A. D. Jara, A. Betemariam, G. Woldetinsae, and J. Y. Kim, "Purification, application and current market trend of natural graphite: A review," International Journal of Mining Science and Technology, vol. 29, Sep. 2019, pp. 671-689, doi: 10.1016/j.ijmst.2019.04.003.
- [7] J. Li, C. Song, Z. Yu, D. Lu, and Y. Cheng, "Status and prospect for purification technology of crystalline graphite," Carbon Techniques, vol. 40, 2021, pp. 15-19, doi: 10.14078/j.cnki.1001-3741.2021.06.003.
- [8] C. Song, J. Li, Z. Yu, D. Lu, and W. Zhang, "Study of Purification Technology of Large Scale Graphite by Plasma," Journal of Heilongjiang University of Technology(Comprehensive Edition), vol. 21, pp. 61-69, 2021, doi: 10.16792/j.cnki.1672-6758.2021.07.012.
- [9] Y. Cheng, Z. Yu, J. Li, C. Song, D. Lu et al., "Study on purification of flaky graphite by argon arc plasma torch," High Power Laser and Particle Beams, vol. 33, 2021, pp. 185-194.
- [10] J. Li, C. Song, D. Lu, R. Huang, and H. Zhang, "Study on plasma spraying graphite purification device," IOP Conference Series: Earth and Environmental Science, vol. 772, no. 1, p. 012070, May 2021, doi: 10.1088/1755-1315/772/1/012070.
- [11] M. Cheng, Y. An, H. Du, Y. Wei, and D. Fan, "Effect of current changes on velocity and temperature profiles of GTAW arc," Transactions of the China Welding Institution, vol. 31, 2010, pp. 33-37+114.
- [12] H. Du, Y. An, Y. Wei, W. Wang, and D. Fan, "Effect of protective gas flow and arc length variations on arc temperature field and flow field," Transactions of the China Welding Institution, vol. 31, 2010, pp. 73-76+116-117.
- T. Chai, Z. Li, L. Feng, and S. Ren, "Numerical Simulation of Arc Properties in Argon and Helium Plasmas," Hot Working Technology, vol. 44, 2015, pp. 175-177+180, doi: 10.14158/j.cnki.1001-3814.2015.05.054.

# International Journal of Multiphysics

Volume 18, No. 2, 2024

ISSN: 1750-9548

- D. Wang, Z. Tian, L. Shen, Z. Liu, and Y. Huang, "Numerical simulation of nanostructured agglomerated powder melting process during plasma spraying," China Mechanical Engineering, vol. 20, 2009, pp. 417-422.
- [15] Y. Zhou, Z. Luo, L Wang, Z. Xia, T. Gao, et al., "Plasma synthetic jet actuator for flow control: Review," Acta Aeronautica et Astronautica Sinica, vol. 43, 2022, pp. 98-140.
- [16] G. Gu and X. Li, "Exponential weighted smoothing prediction model based on boxplot anomaly detection," Computer and Modernization, no. 01, 2021, pp. 28-33.
- [17] G. Yu, "Research on neural network predictive control of decomposing furnace outlet temperature," Master's Thesis, Hefei University of Technology, 2021, doi:10.27101/d.cnki.ghfgu.2021.000957.
- [18] Z. Tang, B. Zhang, S. Cao, G. Wang, and B. Zhao, "Furnace temperature modeling based on multi-model intelligent combination algorithm," CIESC Journal, vol. 70, 2019, pp. 301-310.
- [19] Y. Wang, "Simulation study of neural network predictive control in a sizing system for medium density fiberboards," Master's Thesis, Northeast Forestry University, 2013.
- [20] J. A. Vásquez-Coronel, M. Mora, and K. Vilches, "Training of an Extreme Learning Machine Autoencoder Based on an Iterative Shrinkage-Thresholding Optimization Algorithm," Applied Sciences, vol. 12, no. 18, Sep. 2022, pp. 9021, doi: 10.3390/app12189021.
- [21] I. Manssouri, B. Boudebbouz, and B. Boudad, "Using artificial neural networks of the type extreme learning machine for the modelling and prediction of the temperature in the head the column. Case of a C6H11-CH3 distillation column," Materials Today: Proceedings, vol. 45, Jan. 2021, pp. 7444–7449, doi: 10.1016/j.matpr.2021.01.920.
- [22] S. Shin, J.-U. Won, and M. Kim, "Comparative research on DNN and LSTM algorithms for soot emission prediction under transient conditions in a diesel engine," Journal of Mechanical Science and Technology, vol. 37, no. 6, Jun. 2023, pp. 3141–3150, doi: 10.1007/s12206-023-0538-y.
- [23] A. Massaro, N. Savino, A. M. Galiano, and G. Meuli, "Voice analysis rehabilitation platform based on LSTM algorithm," International Journal of Telemedicine and Clinical Practices, vol. 1, no. 1, Jan. 2020, pp. 1, doi: 10.1504/ijtmcp.2020.10034206.